

Cyclotol Detonation Performance as a Function of Scale and Geometry

Eric K. Anderson and Scott I. Jackson

Los Alamos National Laboratory, Los Alamos, NM, 87545

Abstract. Melt-castable high explosives composed of RDX and TNT are often referred to as Cyclotols. For the present work, we use the term Cyclotol to refer to compositions varying from 75 wt% RDX and 25 wt% TNT to 80 wt% RDX and 20 wt% TNT. In the current effort, we report detonation velocities and front shapes for three different diameter cylindrical rate-sticks. In addition, we report the results of an unconfined slab geometry rate-stick and a copper confined cylinder expansion (CYLEX) test. A relationship between local front curvature and normal velocity is reported for all experiments. In addition, we compute product isentropes from the CYLEX test results and report a product equation of state fitted to this data.

Introduction

Explosives composed of RDX and TNT blends are widely used in explosive munitions, in part due to the fact that they can be melt-casted. A common blend of RDX and TNT is Composition B or Comp B, which nominally contains 60 wt.% RDX and 40 wt.% TNT, and sometimes a small amount of wax¹. Cyclotol is less common in munitions but exhibits higher detonation velocities and product energy due to the higher concentration of RDX².

Computational models that predict detonation performance of an explosive require experimental calibration and validation data. The type of data generally required includes detonation velocity and front-shape measurements over a variety of charge sizes, and, ideally, differing geometries. These measurements are often performed in cylindrical rate-stick experiments, but can also be measured for slab-geometry rate sticks, enabling comparison

with a different geometry. In addition, the detonation performance models attempt to predict the energy delivery characteristics of an explosive. For this reason, experimental measurements of energy release as an explosive detonates are valuable to the development of detonation performance models. An established method of experimentally measuring product energy is the CYLEX test. In this test, a cylindrical explosive charge is placed inside a tube of copper. The motion of the tube wall resulting from detonation of the explosive is measured, and can be analyzed to extract both the total amount of energy released as well as release-rate as a function of time.

In the present work, we report the results of recent Cyclotol detonation experiments where we utilize both cylindrical and slab-shaped charges. In addition, we present results from a cylinder expansion (CYLEX) test scaled to 20 mm inner-diameter (ID). The specific dimensions of the slab were chosen such that release waves emanating from the top and bottom of the charge would not reach the center of the charge before detonation breakout, resulting in a

detonation wave with curvature in one principal dimension rather than two, which is the case for cylindrical rate-sticks. The detonation velocities from the cylindrical tests were previously reported in a previous publication³. Here, we expand on those results and compare them to the slab geometry rate-stick.

In addition to reporting the directly measured detonation performance characteristics (detonation velocities, front-shapes, and CYLEX wall velocities), we report the results of analysis to extract parameters important for HE performance models. These include parameters to describe the $D_n - \kappa$ relationship for the explosive, which are needed for the Detonation Shock Dynamics (DSD) models⁴. Parameters to describe the detonation products using a Jones-Wilkins-Lee (JWL) equation-of-state⁵ are also reported as well.

Experimental

The dimensions and densities of each rate-stick are provided in Table 1. All three unconfined cylindrical rate-sticks were assembled by joining machined 38.1 mm long right-circular cylinders of Cyclotol using a minimal amount of Devcon 5 minute epoxy between pellets. The epoxy was allowed to cure while the rate stick was held in machined v-blocks to ensure accurate alignment.

To measure detonation velocity, the rate sticks were fitted with eleven ionization wires placed in a line along the length of the charge. The wire positions were measured to within $\pm 5 \mu\text{m}$ using an optical comparator. To measure the profile of the detonation front with a streak camera, a PMMA window was placed on the end of the charge. The windows were vapor coated with aluminum to act as a mirror for the streak camera. Illumination provided by an Argon flash charge was directed onto the aluminized PMMA window and imaged using a Cordin 132 streak camera. Additional experimental details on the cylindrical rate-sticks are provided in Kuiper et al.³.

The slab experiment used the same diagnostics as the unconfined cylindrical rate sticks. The slab experiment, however, was constructed using a charge machined from a larger pressing while the cylindrical Cyclotol parts were machined from a melt-casted billet.² A photograph of the completed slab

experiment is shown in Fig. 1.



Fig. 1: Shot 8-1940 assembly. Detonation in the slab was initiated by a Teledyne-Risi RP-2 detonator and a line-wave generator. Ionization wires are visible along the centerline of slab and a font curvature window is at the center of the breakout surface.

Size Effect

Detonation velocities for unconfined Cyclotol as a function of charge radius or thickness are shown in Fig. 2. The experiments in this figure represent tests conducted with RDX/TNT ratios varying from 75/25 to 80/20, and densities varying from 1.738 g/cc to 1.753 g/cc. The 80/20 and 75/25 experiments are shown both with and without a density correction factor to 1.740 g/cc. The blue curve represents the Eyring-form fit to the 77/23 and 80/20 data (blue line)³, with density correction.

Applying the correction to the 75/25 slab experiment shifts the velocity further from the fit to the cylindrical rate-stick data. Differences in velocities can also be attributed to the varying RDX/TNT ratio, with faster velocities expected for higher RDX concentrations, however application of the density correction brings the velocities for the 80/20 and 75/25 experiments to reasonable agreement with the 77/23 fit. This suggests that concentration variations within this range may have relatively small effect.

It should be noted that the slab experiment lies just above the diameter-effect curve for the cylindrical rate-stick data, by an amount typical of the

Table 1: Measured dimensions, densities, and detonation velocities of Cyclotol rate sticks. Cylindrical rate-sticks were composed of 80/20 RDX/TNT while the slab test was composed of 75/25 RDX/TNT.

Test #	Geometry	Confinement	Charge Diameter or Thickness (mm)	Length (mm)	Density (g/cc)	Detonation Velocity (mm/ μ s)	Standard Error (mm/ μ s)
8-1882	Cylinder	None	7.468	228	1.753	8.101	0.0025
8-1878	Cylinder	None	19.96	305	1.752	8.223	0.0047
8-1876	Cylinder	None	25.4	305	1.751	8.255	0.0037
8-1884	Cylinder	Cylex	19.96	267	1.751	8.245	0.0016
8-1940	Slab	None	10.0	130	1.738	8.150	0.0053

scatter observed for the cylindrical rate-sticks, suggesting that Cyclotol may follow $D = 2T$ scaling reasonably closely.

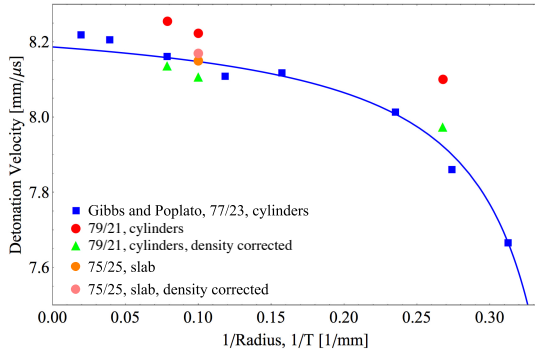


Fig. 2: Los Alamos diameter-effect data for Cyclotol. Composition differences are noted in the legend. Density correction to 1.740 g/cc performed on recent tests to match Gibbs and Poplato¹.

Front Shapes and $D_n - \kappa$ Curves

The Cordin 132 streak camera used to record detonation front-shapes in these experiments is a film camera utilizing a turbine-driven beryllium mirror to direct light onto the film track. To analyze the streak camera records of detonation front-shapes, the film was digitized at 6400 dpi resolution using a film scanner. The resulting digital image was scaled in the horizontal (r) direction and vertical (z) direction. The variable r , corresponds to the radial position on rate stick experiments, or position along the thin (10 mm) dimension of the slab experiment.

For all experiments, horizontal fiducial marks on the experiment were recorded in still images recorded prior to firing the shot, enabling precise r direction scaling.

The vertical direction on the streak camera film represents time during the experiment, and the temporal scaling can be calculated for a given camera-mirror period-of-rotation. The temporal scaling can then be scaled using the detonation phase velocity, D_0 , to distance along the direction of detonation propagation, z .

The scaled experimental front-shapes were then fit using the method-of-least-squares to the form discussed in Hill⁶ and based on the work of Bdzil⁷,

$$z(r) = A \left(\ln \left(\cos \left(\frac{\pi \eta}{2 R_e} r \right) \right) \right), \quad (1)$$

where r is the local position on the line imaged by the streak camera, R_e is the radius of the charge in the case of a cylinder and thickness for the case of a slab, and the parameters A and η are fitting constants constrained such that $0.1 < \eta < 1.0$ and $A < 0$.

The normal velocity D_n and local front curvature κ were then found using the equations

$$D_n = \frac{D_0}{\sqrt{1 + (z')^2}}, \quad (2)$$

$D_n - \kappa$ curves were computed from front shapes measured for the 80/20 and 75/25 experiments of Table 1, and are shown in Fig. 3. Excellent agreement is observed between the experiments for κ values below 0.1 1/mm. Only the two smallest unconfined experiments exhibited curvatures much beyond 0.1 1/mm, where they begin to diverge. It

should be noted, however, that the experimental data to support the $D_n - \kappa$ curves decreases to the right in the figure; the dots on each curve represent equal spacing along the recorded detonation front. As a result, the uncertainty increases to the right.

The black curve represents a preliminary fit to the five experiments of Fig. 2, determined using the method of least squares. The fit quality is good for curvature values up to 0.1 1/mm, where most of the experimental data is available. It should be noted that good agreement is observed between the 75/25 slab experiment (orange) and the 80/20 confined and unconfined cylinders. A small range of curvature was observed for this experiment, however, relative to the cylindrical experiments.

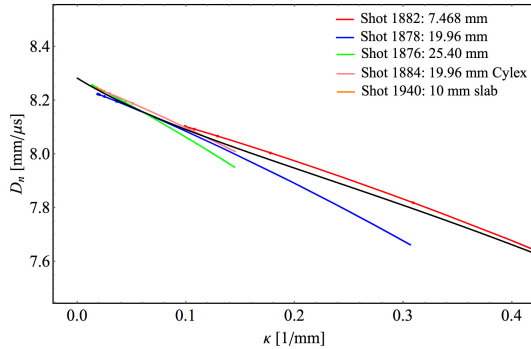


Fig. 3: $D_n - \kappa$ curves computed from detonation velocity and front curvature measurements for the tests of Table 1. The black curve represents a preliminary global fit to all the experiments.

Table 2: Fit to $D_n - \kappa$ curves for Cyclotol 80/20 and 75/25.

Parameter	Values	Units
D_{CJ}	8.282	mm/ μ s
α_1	0.3011	mm
α_2	1.260	mm
α_3	2.240	mm ²
α_4	5.000	mm
α_5	0.000	mm ²

Cylinder Test Results

In this section, the cylinder test wall motion data is presented and analyzed to yield the product isentrope for Cyclotol. The two PDV traces recorded at the standard (2/3 cylinder axial length) are shown in entirety in Figure 4. As discussed previously⁸,

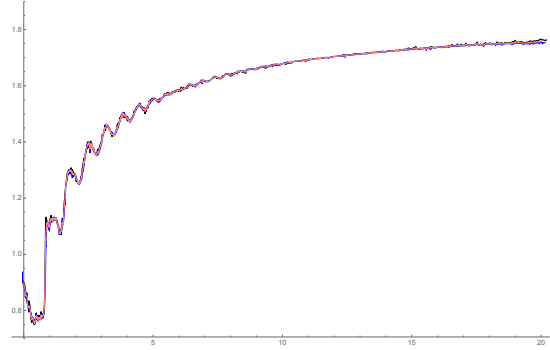


Fig. 4: Full view of the PDV data from test 8-1884. Black and blue curves are the individual PDV measurements at the 2/3 axial length location. The red curve is the average of the individual curves.

the cylinder wall exhibits compressible acceleration, followed by incompressible motion. In the compressible regime, the wall accelerates in a series of pulses or “rings” for the first 7 μ s of motion. After the product pressure drops significantly, the wall motion then transitions into an incompressible regime characterized by smooth acceleration. The wall then fails near 20 μ s, allowing the product gases to escape from the cylinder. Inspection of the PDV data indicates excellent agreement between the two traces over the full test time of the experiment, even during the compressible regime as shown on the zoomed view in Figure 5. For subsequent analysis, the two individual velocity–time curves are averaged and plotted as the red curve in Figures 4 and 5. Fitting this averaged data to the smooth velocity–time equation and parameters listed in ⁹ yields the following fit parameters: $v_\infty = 1.82267$, $a_0 = 1.36414$, and $\omega = 0.858491$.

Previously, it has been shown that the product isentrope can be directly computed from the cylinder wall motion, by using the wall acceleration to infer the product pressure and the cylinder shape to yield the product specific volume^{10, 11, 9, 12}. The

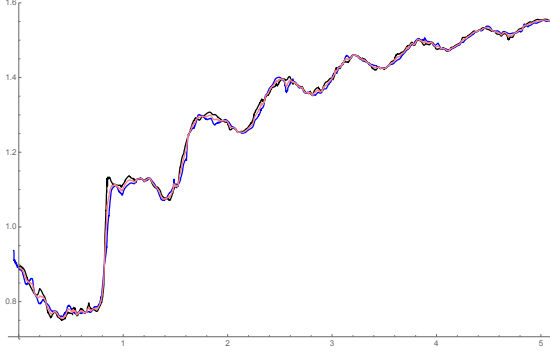


Fig. 5: A zoomed view of the PDV data from test 8-1884, with the color legend the same as Figure 4.

method of ¹¹ (with the correction in ⁹) is used to analyze the average velocity-time motion in both the compressible and incompressible regimes, yielding the black data points shown in Figure 6.

The four highest pressure points are determined from the compressible reduction method using the Copper Hugoniot data discussed in the Appendix, while the remainder are from the incompressible method ¹¹.

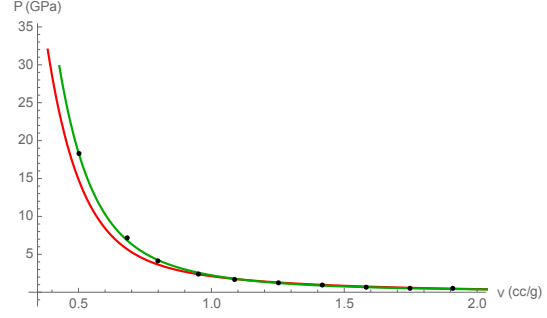
The JWL equation of state (EOS) is an incomplete EOS that is often used to represent detonation product EOS data in a concise analytic form ¹³ The JWL EOS is

$$P(\Delta) = Ae^{-R_1\Delta} + Be^{-R_2\Delta} + C(\Delta)^{-(1+\omega)} \quad (3)$$

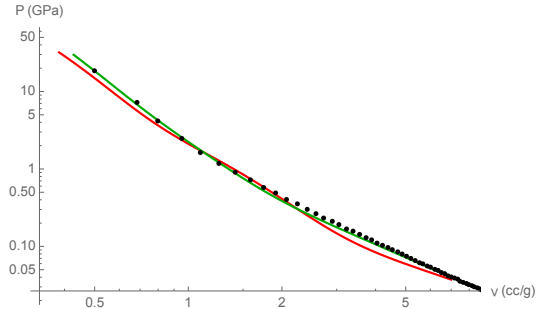
where $\Delta_s = \nu_s/\nu_0$ is the ratio of the product volume to the initial volume. Parameters A , B , C , R_1 , R_2 , and ω are fitted constants. Fitting the present $P-\nu$ data to the JWL form gives the fit parameters in Table 3 with a sonic state of $P_s = 29.8$ and $\nu_s = 0.428$ cc/g.

Our fitting process enforces tangency of the JWL fit with the (one-dimensional) Rayleigh line in $P-\nu$ space at the sonic point ¹³. The fitted form agrees well with the data points in Figure 6, slightly underpredicting them in the low pressure (1-0.1 GPa) regime.

Table 3 also reproduces JWL parameters from earlier Cyclotol cylinder expansion tests discussed in two prior works ^{12, 14}. These JWL curves are plotted against the present data in Figure 7 along with the recently developed empirical correlation model of ¹⁵ that predicts JWL EOS curves using



(a)



(b)

Fig. 6: Product isentrope data as calculated directly from experiment (black points) and for the JWL form fit to this data (green curve). DELETE RED REFERENCE LINE

only ρ_0 and D_0 . Excellent agreement is seen between the present data and the prior work of ¹⁴ and ¹⁵. The JWL of ¹² is lower at high pressures and does not approach the Rayleigh line near the sonic surface.

Appendix

The cylinder expansion test analysis of ¹¹ requires use of the Hugoniot for the cylinder wall material to relate the ringing amplitude to the driving product pressure. The Hugoniot data from ¹⁶ is available for pressures above 8 GPa. There is, however, a dearth of data below this pressure, likely due to limited interest and the complexities of measuring the dynamic pressure in the vicinity of the elastic-plastic region, which we estimate is approx-

Table 3: JWL fit parameters for Cyclotol 77/23 with $\rho_0 = 1.754 \text{ g/cc}$.

JWL Parameters	Present study	Ref. ¹⁴	Ref. ¹²
A (GPa)	948.2	560.0	603.4
B (GPa)	30.7	5.13	9.92
C (GPa)	3.17	1.36	1.08
R_1	5.31	4.12	4.7
R_2	1.97	0.995	1.1
ω	0.74	0.35	0.35
D_0 (mm/ μ s)	8.254	8.250	8.250

imately from 0.2–2 GPa for dead soft copper.

To address this calibration gap, we assume an approximate elastic response for shock-driven copper particle velocities u_p below 0.06 mm/ μ s of the form $P = Eu_p/c_0$ where E and c_0 are Young’s modulus (125 GPa) and the longitudinal sound speed (3.94 mm/ μ s) for Copper, respectively. We then blend this solution with the ¹⁶ Hugoniot trend over $u_p = 0.06$ –0.1 mm/ μ s to ensure data continuity yielding the following low pressure response data: (u_p in mm/ μ s, P in GPa) = (0., 0.), (0.01, 0.317), (0.02, 0.635), (0.03, 0.952), (0.04, 1.269), (0.05, 1.586), (0.06, 1.904), (0.07, 2.288), (0.08, 2.767), (0.09, 3.281), (0.1, 3.829). This data is then combined with the copper Hugoniot data from ¹⁶ and interpolated to relate the ringing velocity response to the product pressure in the compressible regime.

Conclusions

A Cyclotol slab-geometry rate-stick was tested and compared to prior cylindrical rate-stick experiments. The measured detonation velocity was in good agreement with the cylindrical diameter-effect curve using $D = 2T$ scaling. The measured front-shape was used to calculate a $D_n - \kappa$ curve. Again, the slab experiment showed good agreement with the $D_n - \kappa$ curves observed for cylindrical rate-sticks. Based on these results, we believe Cyclotol detonation propagation in room temperature charges can be adequately modeled using simple DSD?

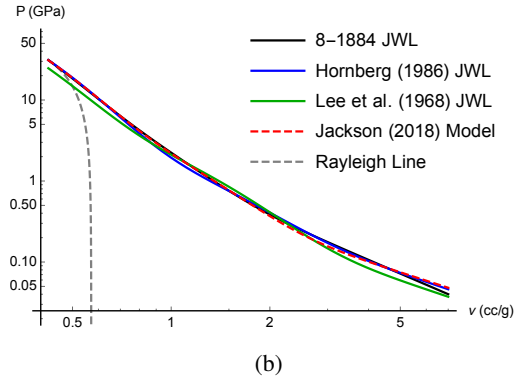
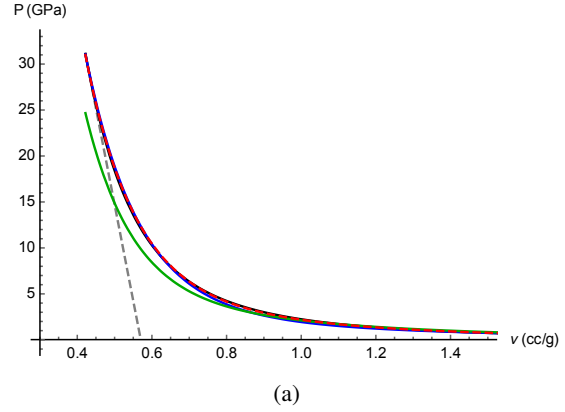


Fig. 7: Comparison of different Cyclotol EOS curves.

References

1. Gibbs, T. R. and Popolato, A., editors, *LASL Explosive Property Data*, Los Alamos Series on Dynamic Material Properties, University of California Press, Berkeley, CA, 1980.
2. Cooper, P., *Explosives engineering*, Wiley-VCH, 1996.
3. Kuiper, T. A., Anderson, E. K., Short, M. and Jackson, S. I., “Detonation performance measurements of cyclotol 80/20,” *AIP Conference Proceedings*, Vol. 1793, pp. 030003–1–030003–5, 2017.
4. Bdzil, J. B. and Stewart, D. S., *Theory of Detonation Shock Dynamics*, pp. 373–453, Springer Berlin Heidelberg, Berlin, Heidelberg, 2012.

5. Lee, E. L., Hornig, H. C. and Kury, J. W., "Adiabatic Expansion Of High Explosive Detonation Products," .
6. Catanach, R. A. and Hill, L. G., "Diameter Effect Curve and Detonation Front Curvature Measurements for ANFO," *AIP Conference Proceedings*, Vol. 620, pp. 906–909, 2002.
7. Bdzil, J. B., "Steady-state two-dimensional detonation," *Journal of Fluid Mechanics*, Vol. 108, p. 195?226, 1981.
8. Jackson, S., "Scaled Cylinder Test Experiments with Insensitive PBX 9502 Explosive," in "Proceedings of the 15th International Detonation Symposium," pp. 171–180, Office of Naval Research, 2015.
9. Jackson, S., "The dependence of Ammonium-Nitrate Fuel-Oil (ANFO) detonation on confinement," *Proceedings of the Combustion Institute*, Vol. 36, pp. 2791–2798, 2017.
10. Taylor, G., "Analysis of the explosion of a long cylindrical bomb detonated at one end," *Mechanics of Fluids, Scientific Papers of G.I. Taylor*, Vol. 2, pp. 277–286, 1941.
11. Jackson, S., "An analytic method for two-dimensional wall motion and product isentrope from the detonation cylinder test," *Proc. Combust. Inst.*, Vol. 35, pp. 1997–2004, 2015.
12. Lee, E., Horning, H. and Kury, J., "Adiabatic expansion of high explosives detonation products," *Technical Report TID 4500-UCRL 50422*, Lawrence Livermore National Laboratory, University of California, Livermore, CA, 1968.
13. Davis, W., "3: Shock Waves, Rarefaction Waves, Equations of State," in "Explosive Effects and Applications," , edited by J.A. Zukas, W. W., chapter 3, pp. 47–112, Springer, 1998.
14. Hornberg, H. and Volk, F., "The cylinder test in the context of physical detonation measurement methods," *Propellants, Explosives, Pyrotechnics*, Vol. 14, pp. 199–211, 1989.
15. Jackson, S. I., "Scaling of the detonation product state with reactant kinetic energy," *Combustion and Flame*, Vol. 190, pp. 240–251, 2018.
16. Marsh, S., in "LASL Shock Hugoniot Data," pp. 57–60, University of California, 1980.